

Supporting Information

A hollow $\text{Co}_{3-x}\text{Cu}_x\text{S}_4$ with glutathione depleting and photothermal properties for synergistic dual-enhanced chemodynamic/photothermal cancer therapy

Ying Jiang¹, Hao Lu¹, Xiangyang Yuan¹, Yuanyuan Zhang¹, Lingli Lei², Yongcan Li¹, Wei Sun⁴, Jing Liu¹, Daniel Scherman^{1,3,*} and Yingshuai Liu^{1,*}

¹Key Laboratory of Luminescence Analysis and Molecular Sensing (Southwest University), Ministry of Education, School of Materials and Energy, Southwest University, Chongqing, 400715, P. R. China. E-mail: ysliu@swu.edu.cn

²Small Molecule Drugs Sichuan Key Laboratory, School of Pharmacy, Chengdu Medical College, Chengdu, 610500, P. R. China.

³Université de Paris, CNRS, INSERM, Faculté des Sciences Pharmaceutiques et Biologiques, UTCBS, Paris, 75006, France.

⁴Key Laboratory of Laser Technology and Optoelectronic Functional Materials of Hainan Province, College of Chemistry and Chemical Engineering, Hainan Normal University, Haikou 571158, P R China.

*Corresponding authors: daniel.scherman@parisdescartes.fr; ysliu@swu.edu.cn

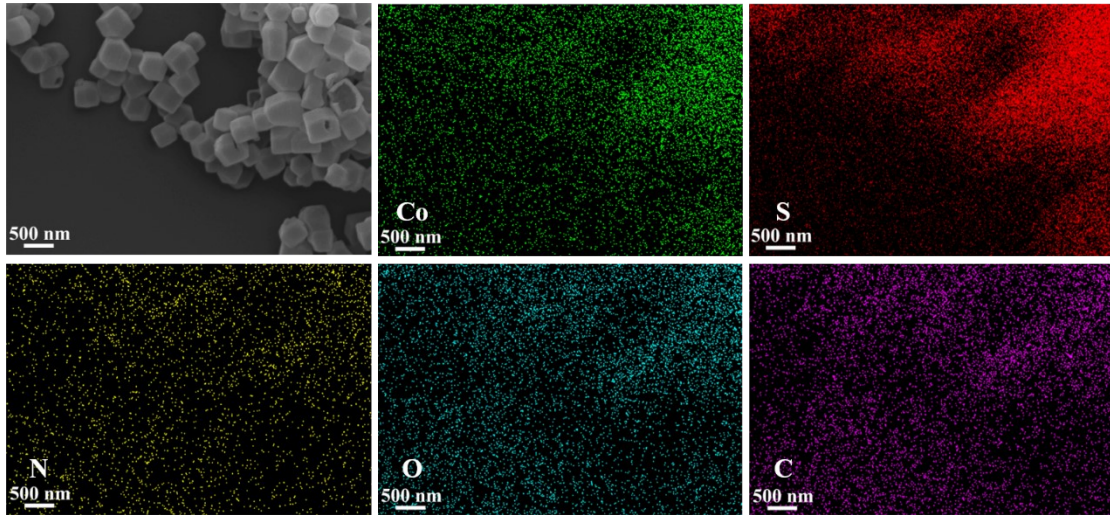


Figure S1. FESEM image and EDS elemental mapping images of Co_3S_4 .

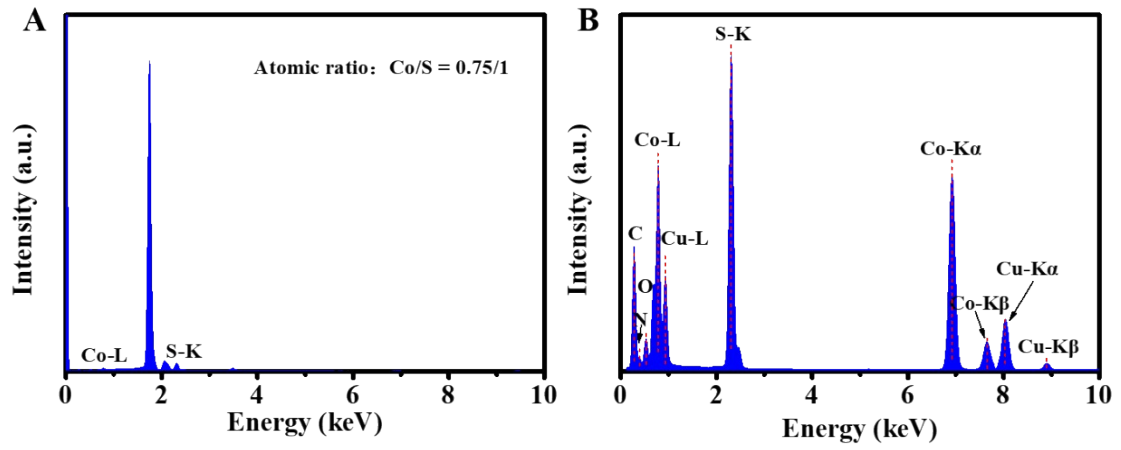


Figure S2. EDS spectroscopy of (A) Co_3S_4 and (B) $\text{Co}_{3-x}\text{Cu}_x\text{S}_4$.

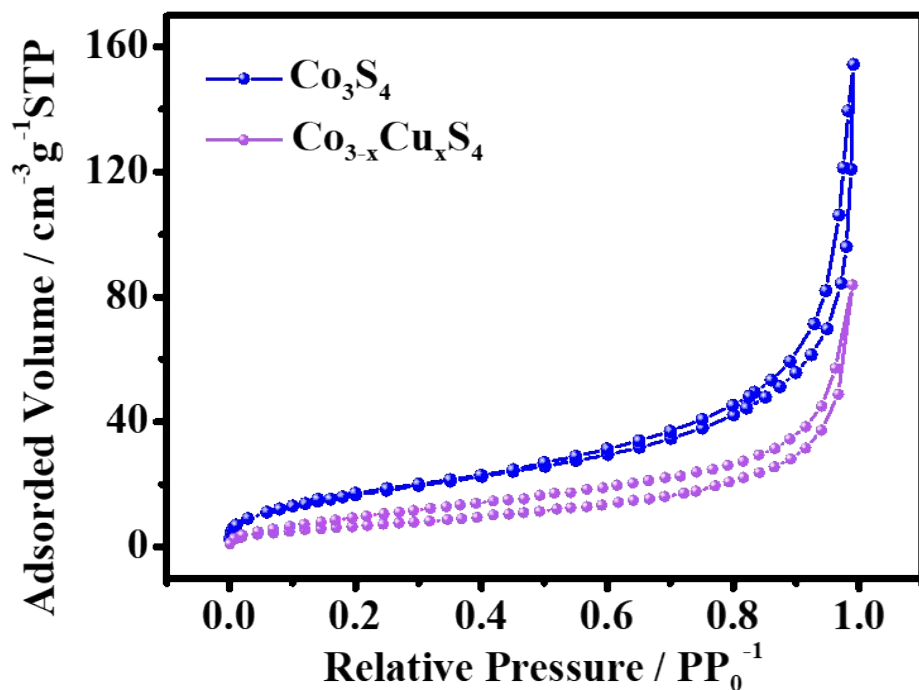


Figure S3. N₂ adsorption-desorption isotherms of Co₃S₄ and Co_{3-x}Cu_xS₄.

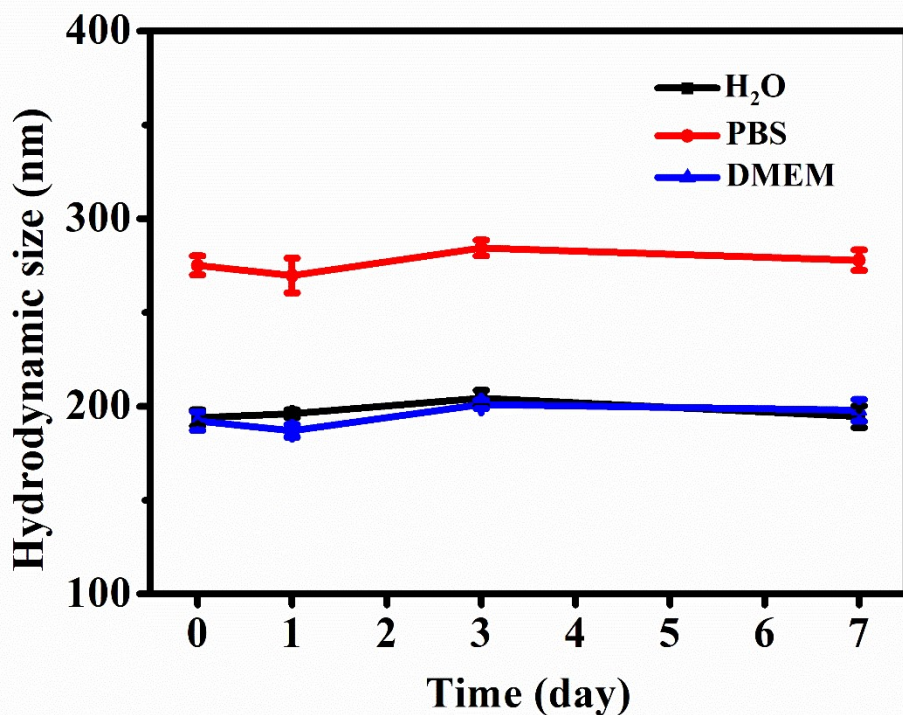


Figure S4. Hydrodynamic size of CCP in various aqueous media.

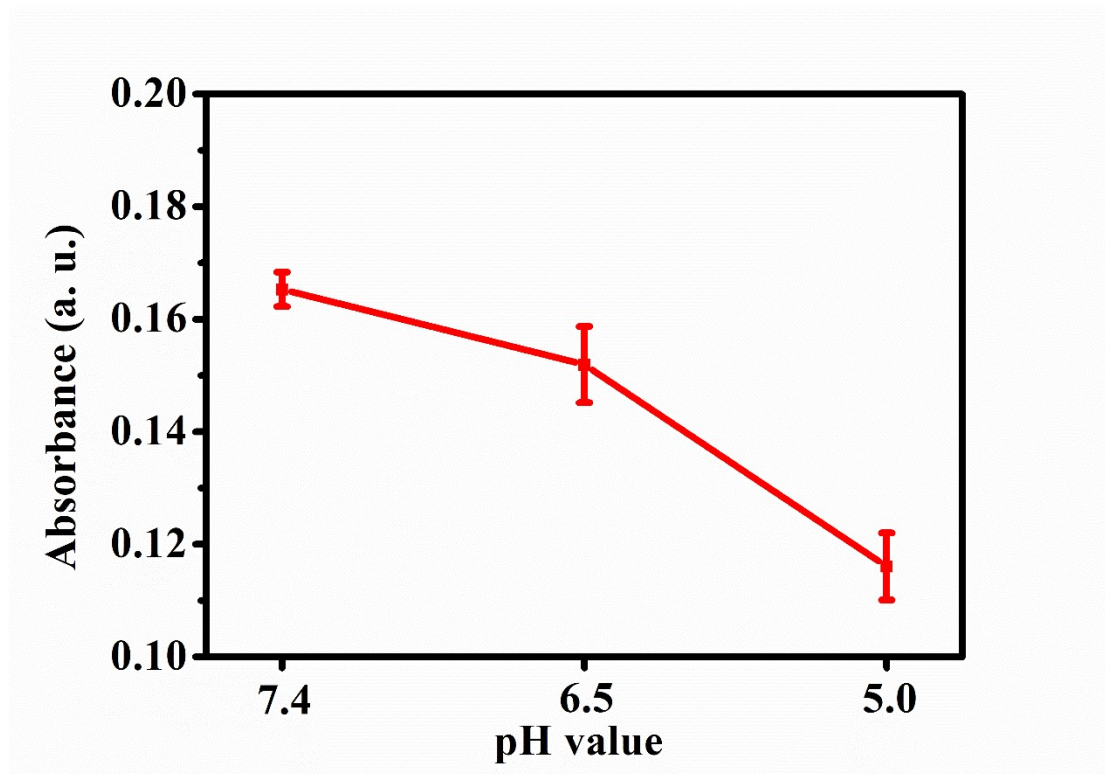


Figure S5. pH-responsive degradation of CCP at various pH values (7.4, 6.5, and 5.0).

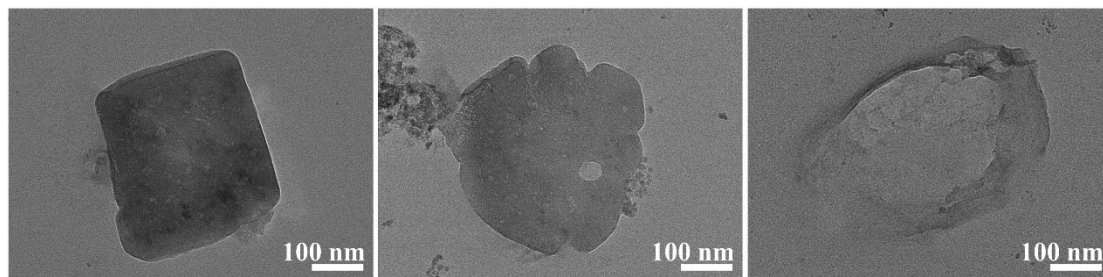


Figure S6. TEM images of CCP after being soaked into PBS with different pH values (7.4, 6.5, and 5.4).

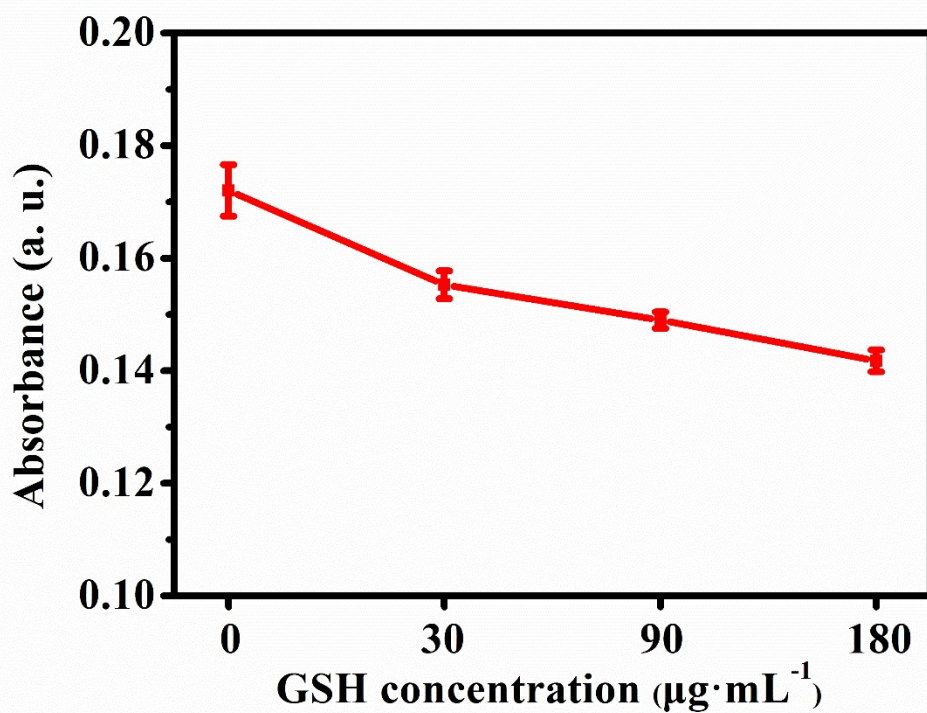


Figure S7. GSH-responsive degradation of CCP.

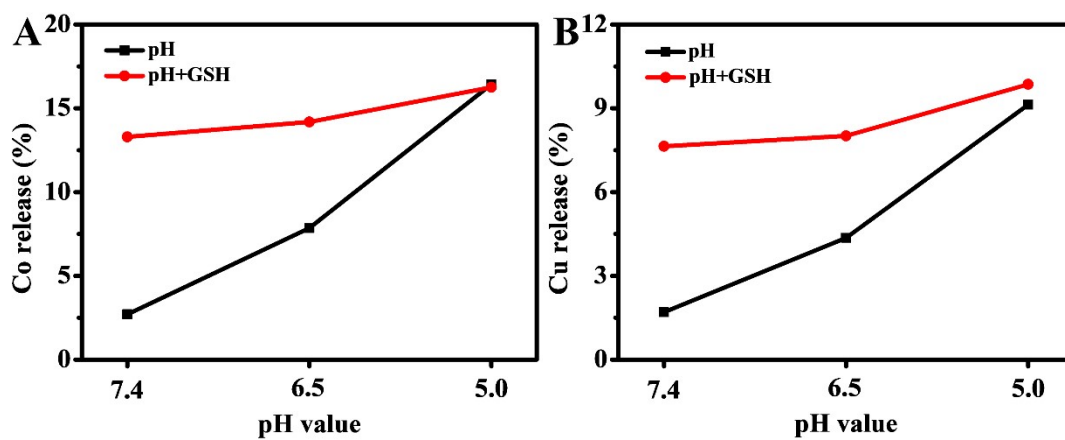


Figure S8. Accumulative Co (A) and Cu (B) release of CCP in PBS solution with different pH values (7.4, 6.5, and 5.0) and in the presence of GSH.

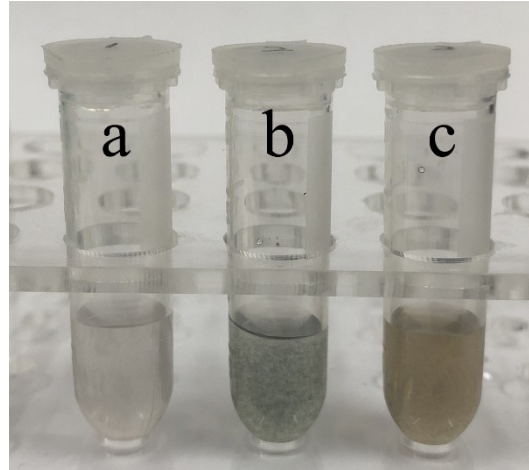


Figure S9. Ammonium hydroxide as an indicator to detect the presence of Cu^{2+} in solution. (a) CCP, (b) CCP+ $\text{NH}_3 \cdot \text{H}_2\text{O}$, (c) CCP+GSH+ $\text{NH}_3 \cdot \text{H}_2\text{O}$.

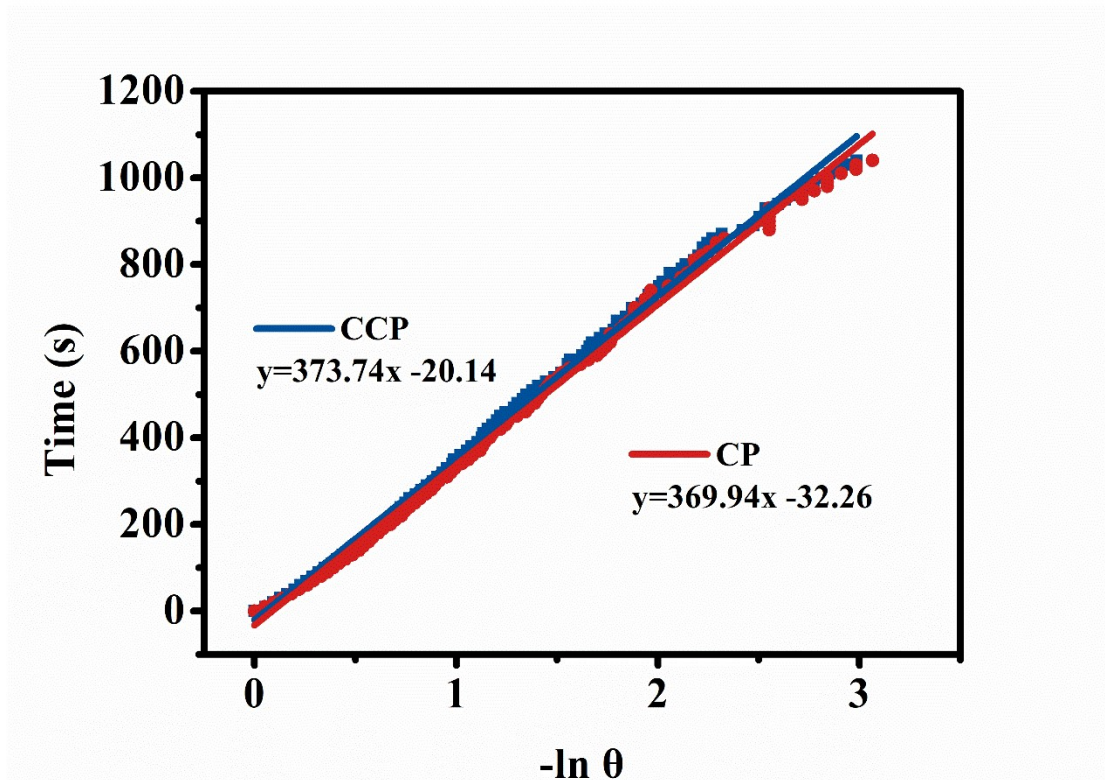


Figure S10. Fitting curve of time as a function of $-\ln(\theta)$ derived from the cooling stage of CP and CCP.

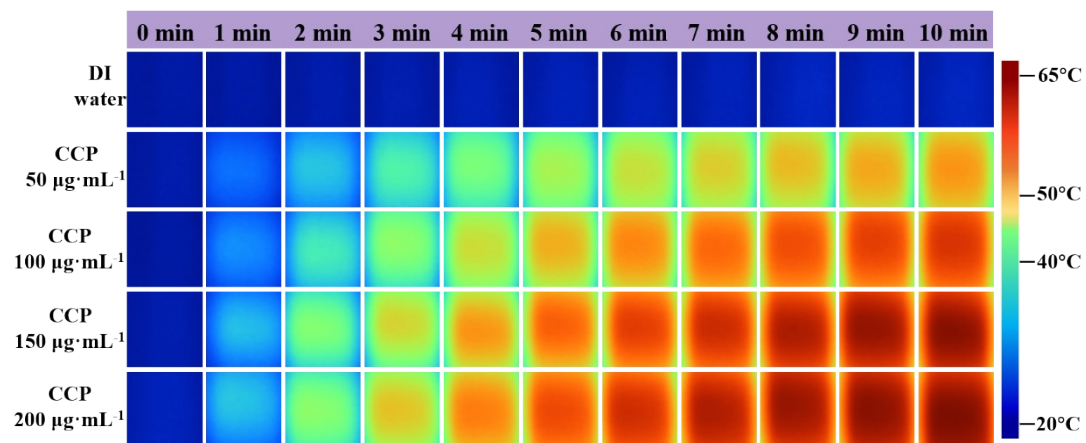


Figure S11. Infrared thermographic images of CCP (0-200 $\mu\text{g}\cdot\text{mL}^{-1}$) under 808 nm laser (1.0 $\text{W}\cdot\text{cm}^{-2}$).

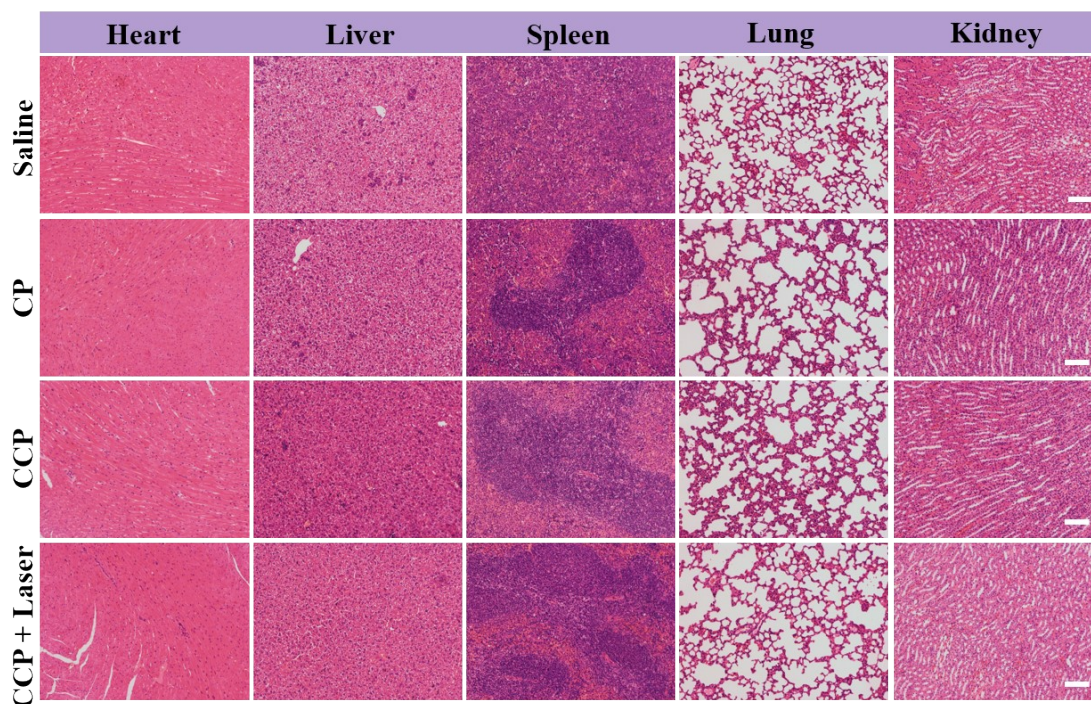


Figure S12. H&E staining histological images of major organs of mice at 14 d post-injection, scale bar: 100 μm .